A full cycle anti-viral drug screen identifies a clinical compound against adenovirus infection

Fanny Georgi[1], Fabien Kuttler[2], Luca Murer[1], Vardan Andriasyan[1], Robert Witte[1], Artur Yakimovich[3,4], Gerardo Turcatti[2], Urs F Greber[1]

[1] Department of Molecular Life Sciences, University of Zurich (UZH), Winterthurerstrasse 190, 8057 Zurich, Switzerland
[2] Biomolecular Screening Facility, School of Life Sciences, Ecole Polytechnique Fédérale (EPFL) de Lausanne, Station 15, Lausanne 1015, Switzerland
[3] MRC Laboratory for Molecular Cell Biology, University College London, Gower St, London, WC1E 6BT, United Kingdom
[4] Artificial Intelligence for Life Sciences CIC, 40 Gowers walk, London, E1 8BH, United Kingdom
Corresponding author: Urs F Greber, urs.greber@imls.uzh.ch

Human adenoviruses (HAdVs) are fatal to immune-suppressed people, but no effective anti-HAdV therapy is available. Here, we present a novel image-based high-throughput screening (HTS) platform, which scores the full viral replication cycle from virus entry to dissemination of progeny. We analysed 1,280 small molecular compounds of the Prestwick Chemical Library (PCL) for interference with HAdV-C2 infection in a quadruplicate blinded format, followed by robust image analyses, and hit identification. We present the entire set of image-based screening data including all the images, and the image analysis and data processing pipelines, as deposited at the Image Data repository (IDR) [1], accession number idr0081. We identified Nelfinavir mesylate as an inhibitor of HAdV plaque formation, in agreement with the previous notion that Nelfinavir is ineffective in single round HAdV infection assays. Nelfinavir has been FDA-approved for anti-retroviral therapy in humans. Our results underscore the power of image-based multi-round infection assays in identifying viral inhibitors with clinical potential.

Background & Summary:

Human adenoviruses (HAdV) predominantly cause diseases of the respiratory and gastrointestinal tracts. They are a significant cause of acute human disease with morbidity and mortality, especially for immuno-compromised patients [2,3] as indicated by a recent outbreak in the USA killing 12 children. Surprisingly, a recent case of HAdV-C2 caused meningoencephalitis was also reported in a middle-aged woman in the US [4]. HAdV have a high prevalence [5–8] and are broadly used as gene therapy vectors [9] and oncolytic viruses [10,11]. The high seroprevalence of HAdV-C2/5 [12] underlines that HAdV infections are asymptomatic in healthy individuals, but HAdV persist in mucosal lymphocytes, and thereby pose a severe risk for immunosuppressed patients undergoing stem cell transplantation [13].

More than 100 HAdV genotypes have been formally approved [14] and are grouped into seven species based on hemagglutination assay and genome sequences [15]. They exhibit a broad range of tissue tropism, including the respiratory and gastrointestinal tracts, the eye, the kidney, the urogenital tracts and blood cells. While species A, F and G target the gastrointestinal tract, HAdV-B, C and E cause infections of the respiratory tract, and conjunctivitis is mostly associated with species B and D, but also C types. HAdV-B show the broadest spectrum of tropisms, also infecting the kidney and hematopoietic system [7,13].

HAdV is a non-enveloped virus with a double-stranded DNA genome of ~36 kbp tightly packaged into an icosahedral capsid of about 90 nm in diameter [16,17]. The best-studied HAdV are HAdV-C2/5 (species C, type 2 and 5), which are very closely related to each other. HAdV enter cells by receptor mediated endocytosis, penetrate the endosomal membrane by the activation of a viral lytic machinery, and shed virion proteins in a stepwise manner, until they arrive at the nuclear membrane, where they uncoat and release their genome to the nucleus [18,19]. In the nucleus the viral genome gives rise to the immediate early viral mRNA encoding the E1A protein which then transactivates all the subviral promoters and is key to give rise to lytic infection and maintains viral persistence in presence of the innate immune regulator interferon [20]. Mature HAdV progeny is known to be released by cell lysis upon rupture of the nuclear envelope and the plasma membrane, giving rise to cell-free virions [21–23].

To this day, no effective anti-viral therapy is available against HAdV infection For example, the nucleoside analogue Cidofovir is the current standard of care for the treatment of HAdV infections, albeit with poor clinical efficacy [7]. Cidofovir is a general inhibitor of viral DNA polymerases and impairs the replication of viral DNA [24]. The pre-clinical development of novel anti-HAdV agents has been limited by the shortage of a suitable small animal model, although Syrian Hamsters support HAdV-C progeny production, albeit in limited amounts [25].

Here, we developed a data-based approach to identify novel inhibitors of HAdV infection by testing the Prestwick Chemical Library (PCL) to inhibit HAdV-C2 infection in cell cultures. The PCL is commercially available, and comprises a library of 1,280 off-patent FDA-approved small molecules (listed in Supplementary Table 1) covering significant pharmaceutical range. PCL has been successfully used to identify many compounds for repurposing applications ranging from antimicrobial agents[26] to anticancer candidates [27]. For a full list of publications, see [28]. We performed a phenotypic screen for HAdV-C2 infection, as outlined in (Figure 1A, 1B). We took advantage of automated fluorescence microscopy and image-based scoring of the progression of multi-round infections using Plaque2.0 software [29]. This high-throughput screening (HTS) modality was carried out at a 384-well plate format. For representative images, see Figure 1C.

We demonstrate robust imaging methodology, image analysis and data processing routines as concluded from parallel procedures in two teams at independent institutions, the Biomolecular Screening Facility at Ecole Polytechnique Fédérale de Lausanne (EPFL) and the Department of Molecular Life Sciences at University of Zurich (UZH). To score the infection phenotypes, we used five infection assay features obtained from microscopy: the number of nuclei, the number of infected nuclei, the infection index as calculated from the total nuclei and the infected cells, the number of plaques (areas of multi-round infection foci originating from a single infected host cell) and the integrated viral infection marker, in this case the green fluorescence protein (GFP) intensity. All data is available at the Image Data repository (IDR) [1] (IDR accession number idr0081). The structure of the repository is outlined in Figure 2. Raw and scored infection phenotype features are shown for UZH and EPFL analyses (Supplementary Tables 2 and 3, and Supplementary Tables 4 and 5, respectively). Rigorous assay development ensured a high assay quality as indicated in Figure 3 and by mean Z'-factors of 0.52 for the number of plaques (Table 1). The screening was performed in four biological replicates at high reproducibility, see Figure 4 and Table 2. We further excluded those PCL compounds that showed significant toxicity in the

absence of infection (Table 3 and Figure 5). Imaging, image analysis and scoring by the two independent teams yielded well correlated scores, as depicted in Figure 6.

Our data indicate a high significance of the identified top hit, Nelfinavir mesylate (Figure 1D and 6). We confirmed the efficacy of Nelfinavir as an inhibitor of HAdV infection by biological follow-up studies (submission in preparation).

Methods:

Virus

HAdV-C2-dE3B virus was produced as described [21]. In brief, the virus was generated by exchange of the viral E3B genome region with a reporter cassette harbouring the enhanced green fluorescent protein (GFP) under the immediate early Cytomegalovirus (CMV) promoter. The virus was grown in A549 cells and purified by double caesium chloride gradient centrifugation [30]. Aliquots supplemented with 10% glycerol (v/v) were stored at -80°C. HAdV-C2-dE3B was found to be homogeneous by SDS-PAGE and negative-stain analyses by transmission electron microscopy.

Cell line

A549 (human adenocarcinomic alveolar basal epithelium) cells were obtained from the American Type Culture Collection (ATCC), Manassas, USA. The cells were maintained in full medium: high glucose Dulbecco Modified Eagle Medium (DMEM; Thermo Fisher Scientific, Waltham, USA) containing 7.5% fetal bovine serum (FBS, Invitrogen, Carlsbad, USA), 1% L-glutamine (Sigma-Aldrich, St. Louis, USA) and 1% penicillin streptomycin (Sigma-Aldrich, St. Louis, USA) and subcultured following PBS washing and trypsinisation (Trypsin-EDTA, Sigma-Aldrich, St. Louis, USA) weekly. Cell cultures were grown at standard conditions (37°C, 5% CO_2, 95% humidity) and passage number limited to 20.

Preparation of pre plates

10 µl 0.0125% DMSO in PBS was spotted on all 384 wells each of imaging-compatible 384-well plates (Matrix plates #4332, Thermo Fisher Scientific, Waltham, USA) using a Matrix WellMate dispenser and normal bore Matrix WellMate tubing cartridges (Thermo Fisher Scientific, Waltham, USA). Plates were sealed and stored at -20°C.

Blinding

The PCL compound arrangement as spotted by EPFL across the 4 plates A - D comprising each screening set replicate 1 - 4 was blinded and replaced by UZH with internal identifier (Supplementary Tables 2 and 3, *compoundIdentifier* 1 to 1280). The identity of the compounds was only disclosed (Table 3 and Supplementary Tables 1 and 2, *PCL_ID* Prestw-1 to Prestw-1804 and *compoundName*) after the screening process including hit filtering was finished.

Compounds

The PCL was obtained from Prestwick Chemical (Illkirch, France). 3′-Deoxy-3′-fluorothymidine (DFT, CAS number 25526-93-6) was obtained from Toronto Research Chemical, North York,

Canada. All compounds were dissolved in Dimethyl sulfoxide (DMSO, Sigma-Aldrich, St. Louis, USA) at a final stock concentration of 10 mM and stored at -20°C.

Presto-blue toxicity assay

Toxicity of the PCL chemical compounds on A549 in absence of infection was tested using compound concentrations, treatment timing and seeding cell numbers corresponding to the screening protocol, and using the Presto Blue Cell Viability reagent (Thermo Fisher Scientific, Waltham, USA). Briefly, following 3.5-day continuous treatment of A549 cells, 10% final PrestoBlue was added to each well and incubated for 1 h at standard cell incubation conditions. Fluorescence intensity (bottom-read) was then measured using a multi-well plate reader (Tecan Infinite F500, Tecan, Männedorf, Switzerland) with excitation at 560/10 nm, emission at 590/10 nm at a fixed gain. Doxorubicin hydrochloride (Prestw-438, Prestwick Chemical, Illkirch, France) was used as a positive control for cytotoxicity, at a final concentration of 10 µM, and the corresponding volume of DMSO was used as a negative control. The full PCL library was tested on duplicated plates. The EPFL-BSF in-house Laboratory Information Management System (LIMS) was used for data processing and statistical validation. First, raw PrestoBlue readings were normalized per plate to negative control values at 0 and positive controls at 1. Then, the normalized values of the duplicates were averaged. Assay quality was assessed for each plate through the Z'-factor calculation. Compounds were considered toxic hits when the normalized value for all replicates was higher than the average + 3σ (standard deviation, SD) of the DMSO negative control for the corresponding plate. Scores and score SD were then calculated for hit compounds by averaging normalized value for all replicates.

Preparation of Z' and screening plates

10 nl of 10 mM PCL compounds, the nucleoside analogue DFT positive control (all dissolved in DMSO) and DMSO only as negative control were pre-spotted on imaging-compatible 384-well plates (Falcon plates, Corning Inc., New York, USA) using an Echo acoustic liquid handling system (Labcyte, San Jose, USA) by the EPFL-BSF, sealed and stored at -20°C. Z' plates consisted of 192 technical replicates of positive and negative control, each, per 384-well plate. Each screening plate set consisted of 4 plates A to D. Each screening plate consisted of 32 technical replicates of positive and negative control, each, and 320 single technical replicate PCL compounds.

Wet-lab screening pipeline

The screening was performed in four independent biological replicates. Wet-lab liquid handling was performed using a Matrix WellMate dispenser and Matrix WellMate tubing cartridges (Thermo Fisher Scientific, Waltham, USA). Prior to usage, tubings were rinsed with 125 ml autoclaved ddH_2O followed by 125 ml autoclaved PBS. Pre-spotted compound plates were thawed at room temperature (RT) for 30 min, briefly centrifuged before compounds were dissolved in 10 µl/ well PBS. 4,000 A549 cells/ well in 60 µl full medium were seeded onto the compounds using standard bore tubing cartridges. Following cell adhesion over night, the cells are inoculated with $1.77*10^5$ genome equivalents per well of HAdV-C2-dE3B in 10 µl full media using bovine serum albumin (BSA, cell-culture grade, Sigma-Aldrich, St. Louis, USA)-blocked small bore tubing cartridges. Final compound concentration was 1.25 µM at 0.0125% DMSO. Infection was allowed to progress over multiple infection rounds for 72 h giving rise to foci of infected cells originating from a single

first round infected cell termed plaque. Cells were fixed for 1 h at RT by addition of 26.6 µL 16% PFA and 4 µg/ml Hoechst 33342 (Sigma-Aldrich, St. Louis, USA) in PBS using standard bore tubing cartridges. Cells were washed 3 times with PBS before PBS supplemented with 0.02% N_3 was added and plates were sealed for long-term storage at 4°C. Following usage, tubings were rinse with 125 ml autoclaved ddH_2O followed by 125 ml autoclaved PBS and autoclaved for re-usage.

Imaging

Nuclei (DAPI channel) and viral GFP (FITC channel) were imaged on two devices. At UZH, plates were imaged on an IXM-C automated high-throughput fluorescence microscope (Molecular Devices, San Jose, USA) using MetaXpress (version 6.2, Molecular Devices, San Jose, USA) and a 4x air objective (Nikon S Fluor, 0.20 NA, 15.5 mm WD, Nikon Instruments, Minato, Japan) at widefield mode. Image size $2{,}048^2$ px at 1.72 µm/px resolution acquired on an Andor sCMOS camera (Oxford Instruments, Abingdon, UK). Exposure times: DAPI 150 ms, FITC 20 ms. At EPFL, images were acquired on a IN Cell 2200 automated high-throughput florescence microscope (GE Healthcare, Chicago, USA) using IN Cell Analyzer (version 6.2, GE Healthcare, Chicago, USA) and a 4x air objective (Nikon Plan Apo, 0.20 NA, 15.7 mm WD, Nikon Instruments, Minato, Japan) at widefield mode. Image size $2{,}048^2$ px at 1.625 µm/px resolution acquired on an Andor sCMOS camera. Exposure times: DAPI 300 ms, FITC 40 ms.

Image analysis

The infection phenotype for each well was quantified by Plaque2.0 [29] (https://github.com/plaque2/matlab/tree/antivir) via five read-outs: number of nuclei, number of infected nuclei, the ratio between infected and total nuclei referred to as infection index, number of multi-round infection foci termed plaques (plaque forming units, pfu) and the integrated viral transgenic GFP intensity. Plaque2.0 parameters were optimized independently at UZH and EPFL for the data acquired at the respective institution.

Z'-factor calculation

The Z'-factor was computed using R version 3.3.2 [31] according to Equation (1)

$$Z' = 1 - \frac{(3\sigma_+ + 3\sigma_-)}{|\mu_+ - \mu_-|} \quad (1)$$

where σ_+ is the SD of the positive control, σ_- is the SD of the negative control, μ_+ the mean of the positive control and μ_- the mean of the negative control.

Screening data processing

Plaque2.0 results were further independently processed and filtered. At UZH, results were processed in R version 3.3.2 [31], EPFL used KNIME version 3.4.0 [32] as well as the EPFL-BSF in-house LIMS. Mean infection scores over the Plaque2.0 read-outs of the four biological replicates of each PCL compound and the 16 biological replicates containing each 16 technical replicates of positive and negative control, each, were calculated. Each compound's scores were normalized by the mean score of the DMSO negative control of the respective plate. Only non-toxic, effective PCL compounds were considered as HAdV inhibitor candidates. Non-toxic compounds were filtered by applying an inclusive μ_+ (mean of the negative control) $\pm$ 2σ (SD of the negative control) threshold for number of nuclei. Efficacy was filtered by applying an excluding $\mu_+ \pm 3\sigma$ threshold

for the infection scores (number of infected nuclei, infection index, number of plaques or integrated GFP intensity).

Data Records:

Data structure and repository

The HAdV screening data comprise the information collected during assay development, including stability, quality and the PCL screening itself. The latter two have been imaged on two different microscopes. We provide the parameters used for Plaque2.0 image analysis, and the code for the subsequent hit filtering in R. The data structure as available at the IDR [1] , accession number idr0081, is outlined in Figure 2.

Data sets and file types

The provided data consists of four data sets 1 to 4.

- *1-prePlates* contains layouts (.csv), images (.tif), Plaque2.0 image analysis parameters (.mat) and results (.csv) for the assay stability test plates performed at UZH prior to Z' plates (*preZ*) and the AntiVir screen (*preScreen*).
- *2-ZPlates* contains layouts (.csv), images (.tif), Plaque2.0 image analysis parameters (.mat) and results (.csv) for the two Z' plates a and b as imaged and analysed at (*Data_UZH*) and EPFL (*Data_EPFL*).
- *3-Screen* contains layouts (.csv), images (.tif), Plaque2.0 image analysis parameters (.mat) and results (.csv) for the 16 screening plates (4 biological replicas 1 - 4 each consisting of a set of 4 plates A - D) as imaged and analysed at UZH (*Data_UZH*) and EPFL (*Data_EPFL*). Moreover, *Analysis* contains the Plaque2.0 batch processing (*AntiVir_batchprocessing.m*) and hit filtering pipeline (*AntiVir_hitfiltering.R*) used by UZH.
- *4-Toxicity* contains the Presto-blue raw results (.csv) for toxicity in absence of infection.

Technical Validation:

Assay stability

The wet-lab screening pipeline was optimized regarding liquid handling, cell seeding, virus inoculum, positive and negative control, time line, imaging and image analysis to ensure high assay stability and reproducibility. Furthermore, all compounds, especially media and supplements, the BSA for tubing saturation, PFA- and Hoechst-supplemented fixative were prepared as large batch from a single LOT and stored as single-use aliquots. Assay stability with respect to cell and infection phenotype was tested following the established wet-lab, imaging and image analysis pipeline prior to every experiment on pre plates. Since the solvent control had already been spotted in 10 µl PBS, no further PBS was added prior to cell seeding. If infection scores were found to be low due to limited stability of viral stocks, the virus stock dilution in the subsequent experiment was decreased.

Independent analysis

Imaging, image analysis and screening data processing was performed by two independent research teams from two independent institutions at UZH and EPFL. Both dry-lab pipelines confirmed the high assay quality (Table 1). As summarized in Figure 6 left panel, both scores are

strongly correlated with R^2 between 0.6870 - 0.9870. Both approaches yielded identical top scored compounds (Figure 6 right panel), of which Prestw-1764, Nelfinavir mesylate, was the top hit.

Assay quality determination: Z'-factor

The assay's effect size was assessed following the established wet-lab, imaging and image analysis pipeline for two independently performed Z' plates (Table 1 and Figure 2). 3σ Z'-factors of *numberOfInfectedNuclei*, *infectionIndex* and *numberOfPlaques* were in the range of 0.30 to 0.57 and thus good to excellent. *totalVirusIntensity* (Z'-factors between -0.07 to 0.08) are not suitable to identify HAdV infection inhibitors, while *numberOfNuclei* (Z'-factors between -1.11 to -8.10) is not relevant either. Additionally, the Z'-factors were determined for each of the 16 screening plates (Table 2 and Figure 3). 3σ Z'-factors of *numberOfInfectedNuclei*, *infectionIndex* and *numberOfPlaques* were again good to excellent (0.27 to 0.57).

Usage Notes:

Infection scoring using the Plaque2.0 GUI

A detailed manual for Plaque2.0-based infection phenotype scoring is available at http://plaque2.github.io/. No MATLAB license is necessary.

Five parameters were quantified for each well: the number of nuclei (*numberOfNuclei*), number of infected nuclei (*numberOfInfectedNuclei*), the ratio between number of infected and total nuclei (*infectionIndex*), the number of multi-round infection foci termed plaques (*numberOfPlaques*) and the extend of viral GFP reporter expression as integrated GFP intensity *totalVirusIntensity*).

To analyse the HAdV screening data by Plaque2.0, the following setting should be used:

Input/Output:

Processing Folder: Path to folder containing the images (e.g. *ScreenA /3-Screen/Data_EPFL/Screen/ BSF018292_1A*).

filename pattern Data_UZH: *.* (?<wellName>[A-Z][0-9]*)_(?<channelName>w[0-9]*).TIF*

filename pattern Data_EPFL: *.* (?<wellName>[A-Z] - [0-9]+)[(]fld 1 wv (?<channel>[A-Z]{4}) .*.tif*

Plate name: Name of the plate to be analysed (e.g. *BSF018292_1A*)

Result Output Folder: Path to the results folder in the respective Data folder (e.g. *ScreenA/3-Screen/Data_EPFL/Results*).

Stitch: Stitching of the images is not necessary, since every 384-well is imaged in a single site. Do not activate the tab.

Mask:

Custom Mask File: Path to the manually defined mask file (e.g. *ScreenA/3-Screen/Data_UZH/Parameters*).

Monolayer:

Channel: Nuclei were imaged in channel 1.

Plaque:

Channel: Viral GFP reporter signal was imaged in channel 2.

Code Availability:

Plaque2.0 batch image analysis for infection scoring

The MATLAB (version R2016b, The MathWorks, Natick, USA) script *AntiVir_batchprocessing.m* used by UZH for image analysis is provided at IDR, accession number idr0081, under *ScreenA/3-Screen/Analysis*. It is based on the Plaque2.0 software available on GitHub under GPLv3 open source license: https://github.com/plaque2/matlab.

To batch analyse the HAdV screening data by Plaque2.0, fork or download the Plaque2.0 AntiVir code from GitHub: https://github.com/plaque2/matlab/tree/antivir. Place the *AntiVir_batchprocessing.m* file from *ScreenA/3-Screen/Analysis* into the *Plaque2/matlab* folder and follow the instructions in *AntiVir_batchprocessing.m*. A MATLAB license is required.

Hit filtering using R

The R[31] (version 3.6.1 (2019-07-05)) script *AntiVir_hitfiltering* used by UZH for data processing and hit filtering is provided at IDR accession number idr0081 under *ScreenA/3-Screen/Analysis*.

Acknowledgements, Author Contributions & Competing Interests

Author Contributions:

UFG, VA, AY conceived the screening idea. FG designed the experiments, and with UFG coordinated the project. FK prepared the PCL-spotted plates. FG and RW performed the experiments. FG and FK acquired the data. FG and VA analysed the imaging data. LM and FG processed the data. GT organized and supervised the screening project at the EPFL-BSF. FG, FK and UFG wrote manuscript, with input from all the co-authors.

Acknowledgements:

We thank the entire Greber lab for fruitful discussions and critical assessment of the data.

Competing Interests:

The authors declare no conflict of interest.

Funding:

The work was supported by the Swiss National Science Foundation to UFG (Grant numbers 316030_170799 / 1 and 31003A_179256 / 1), and to GT (National Research Program “NCCR chemical biology”).

Abbreviations:

BSA, bovine serum albumin;
BSF, Biomolecular Screening Facility;
CMV, Cytomegalovirus;
DFT, 3′-Deoxy-3′-fluorothymidine;
DMEM, Dulbecco Modified Eagle medium;
DMSO, Dimethyl sulfoxide;
dpi, days post infection;
EPFL, Ecole Polytechnique Fédérale de Lausanne;
FBS, fetal bovine serum;
GFP, green fluorescent protein;
HAdV, Human adenovirus;
hpi, hours post infection;
HTS, high-throughput screening;
IDR, The Image Data Resource;
LIMS, Laboratory Information Management System;
LUT, Look up table;
PCL, Prestwick Chemical Library;
PFA, para-formaldehyde;
pfu, plaque forming units;
RT, room temperature;
SE, standard error;
SD, standard deviation;
UZH, University of Zurich

374 **Figures & Tables**

A

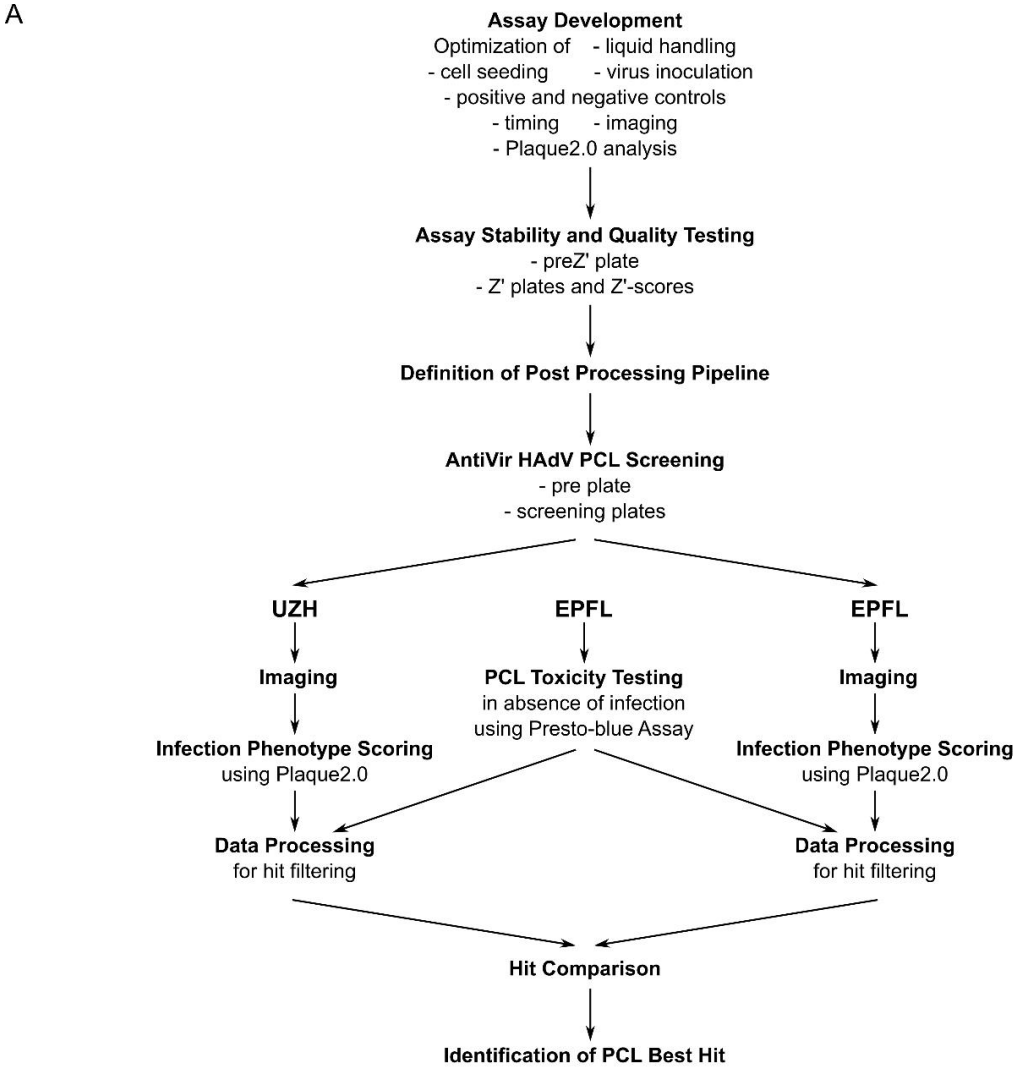

B

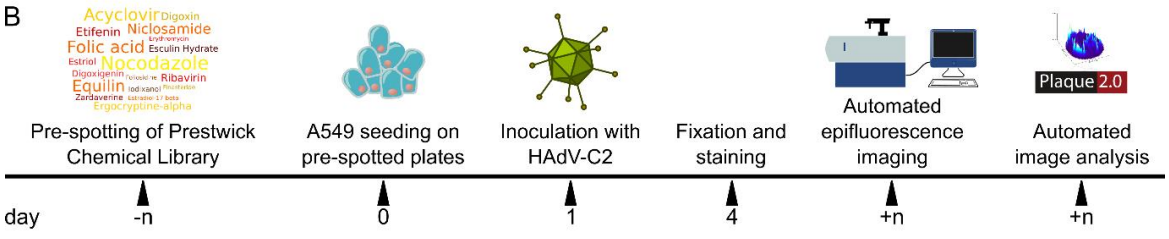

C

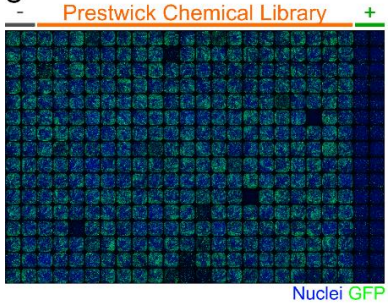

D

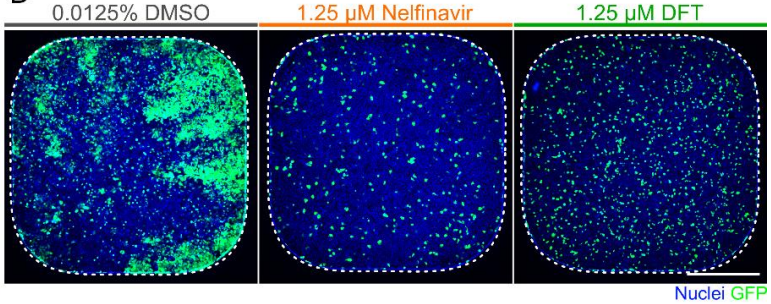

375

Fig. 1: The HAdV screening procedure. A Following assay development, stability and quality testing, the HAdV screening of the PCL is performed. Imaging, image analysis and data processing is performed independently at UZH and EPFL, before ranked hits are compared. **B** Schematic overview of the wet-lab pipeline. PCL compounds and DFT positive control in DMSO as well as DMSO alone as negative control are pre-spotted onto 384-well imaging plates by Echo acoustic liquid handling at 10 nl corresponding to a final concentration of 1.25 µM in 80 µl assay volume/ well and stored at -20°C. Compound-blinded plates are thawed and 4,000 A549 cells/ wells seeded. The following day, the cells are inoculated with HAdV-C2-dE3B at $1.77*10^5$ genome equivalents / well. Allowing for multiple viral replication rounds, the cells are PFA-fixed at 72 hpi and the nuclei stained using Hoechst. The infection phenotype is imaged using an epifluorescence HT microscope and scored using Plaque2.0. The data of the four technical replicates is further processed in R or through EPFL-BSF LIMS. **C** Exemplary epifluorescence microscopy 384-well images stitched to a screening plate overview of consistent of 16 replicates of negative (two most left columns) and positive control (two most right columns) and 320 blinded PCL compounds (centre 20 columns). Hoechst-stained nuclei are shown in blue, viral GFP in green. **D** Representative 384-well epifluorescence microscopy images of the DMSO negative control (most left), the DFT positive control (most right) and the top hit Nelfinavir mesylate (centre). Hoechst-stained nuclei are shown in blue, viral GFP in green. Scale bar is 5 mm.

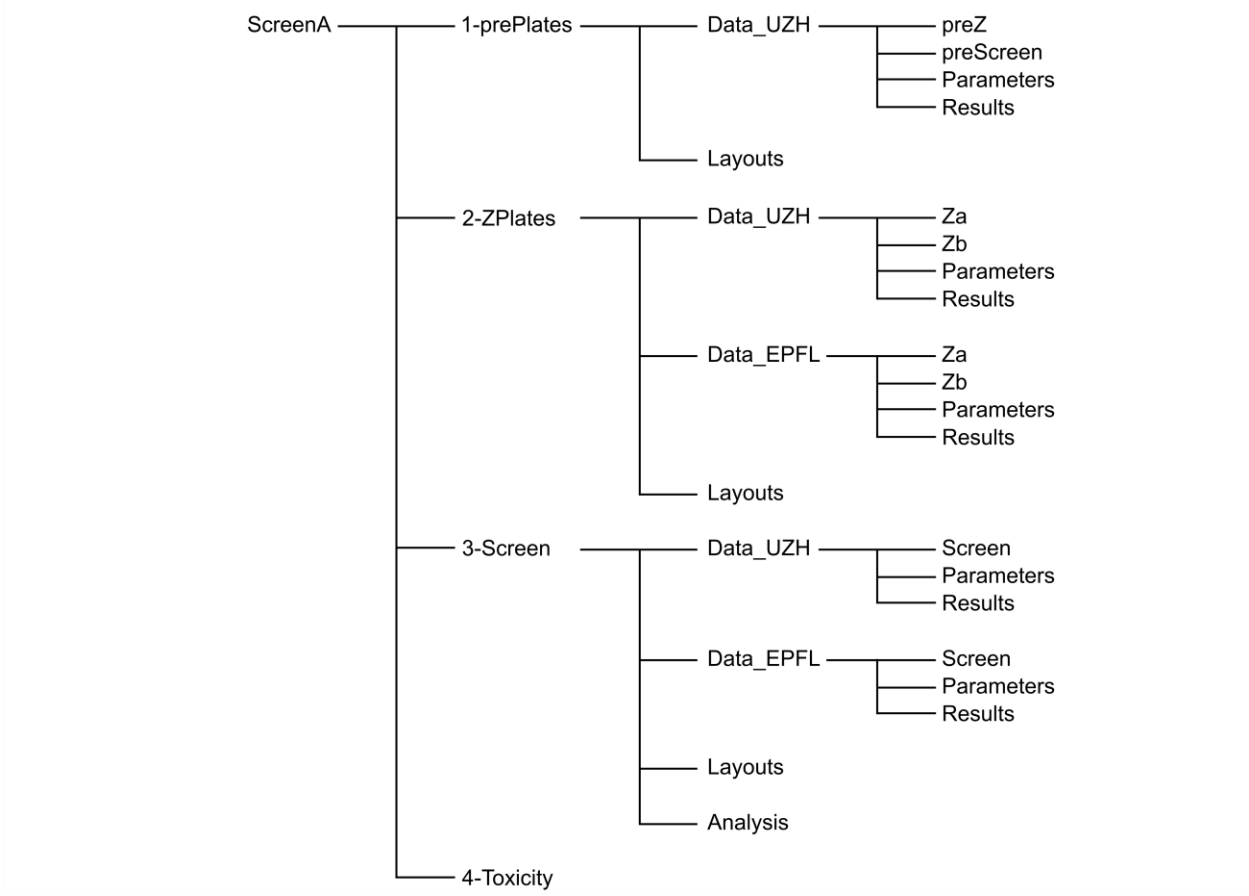

Fig. 2. HAdV data structure as provided at IDR, accession number idr0081.

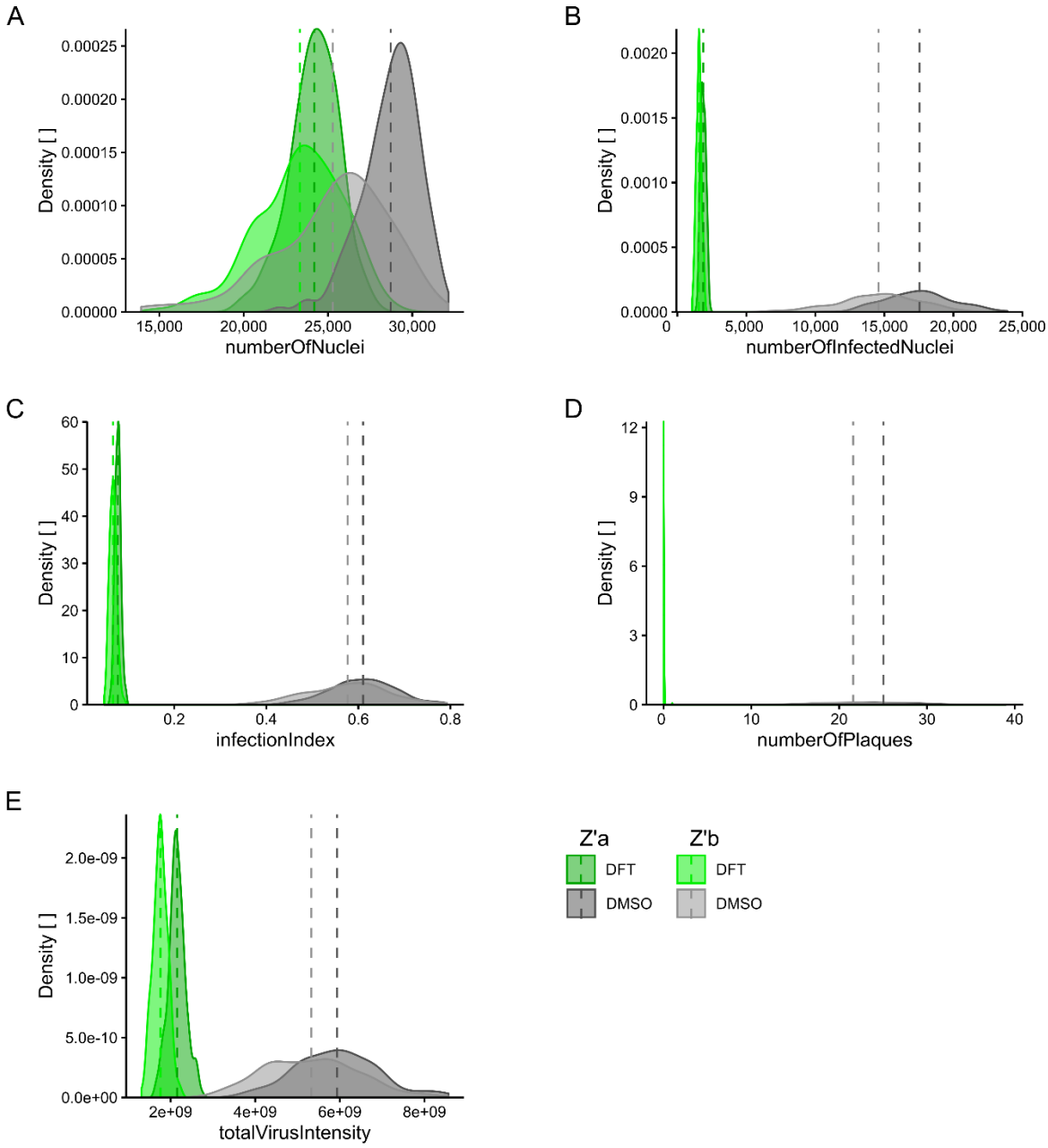

Fig. 3: Infection score density of positive and negative controls across Z' plates. Distribution of **A** *numberOfNuclei,* **B** *numberOfInfectedNuclei*, **C** *infectionIndex*, **D** *numberOfPlaques* and **E** *totalVirusIntensity* in negative control (0.0125% DMSO) compared to positive control-treated (1.25 µM DFT) samples of the two Z' plates. Dark green and dark grey indicates Z' plate a, light green and grey show Z' plate b. Dashed vertical lines mark mean of 192 technical replicas.

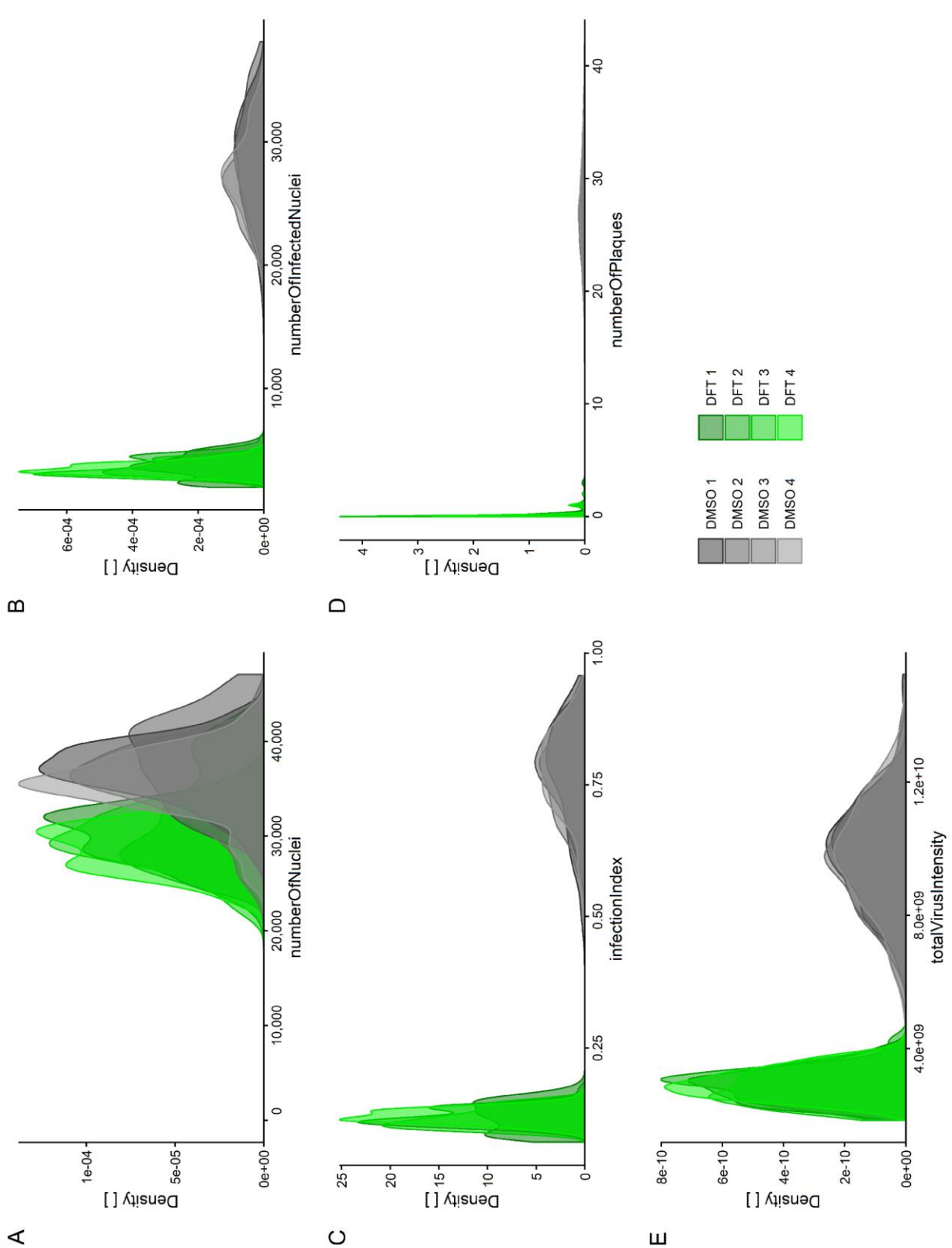

Fig. 4: Infection score density of positive and negative controls across screening replicates. Distribution of **A** *numberOfNuclei,* **B** *numberOfInfectedNuclei*, **C** *infectionIndex*, **D** *numberOfPlaques* and **E** *totalVirusIntensity* in negative control (0.0125% DMSO in grey) compared to positive control-treated (1.25

405 μM DFT in green) samples of the screening sets. Each set 1 to 4 indicated by colour shading is comprised
406 of four plates containing 32 technical replicas per control.

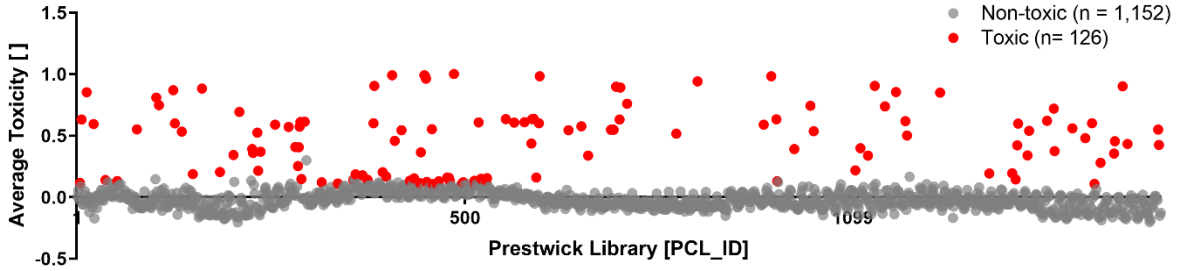

Fig. 5: PCL Toxicity in absence of infection. Of the 1,278 PCL compounds tested, 126 PCL compounds (shown in red, listed in Table 3) are found to be toxic.

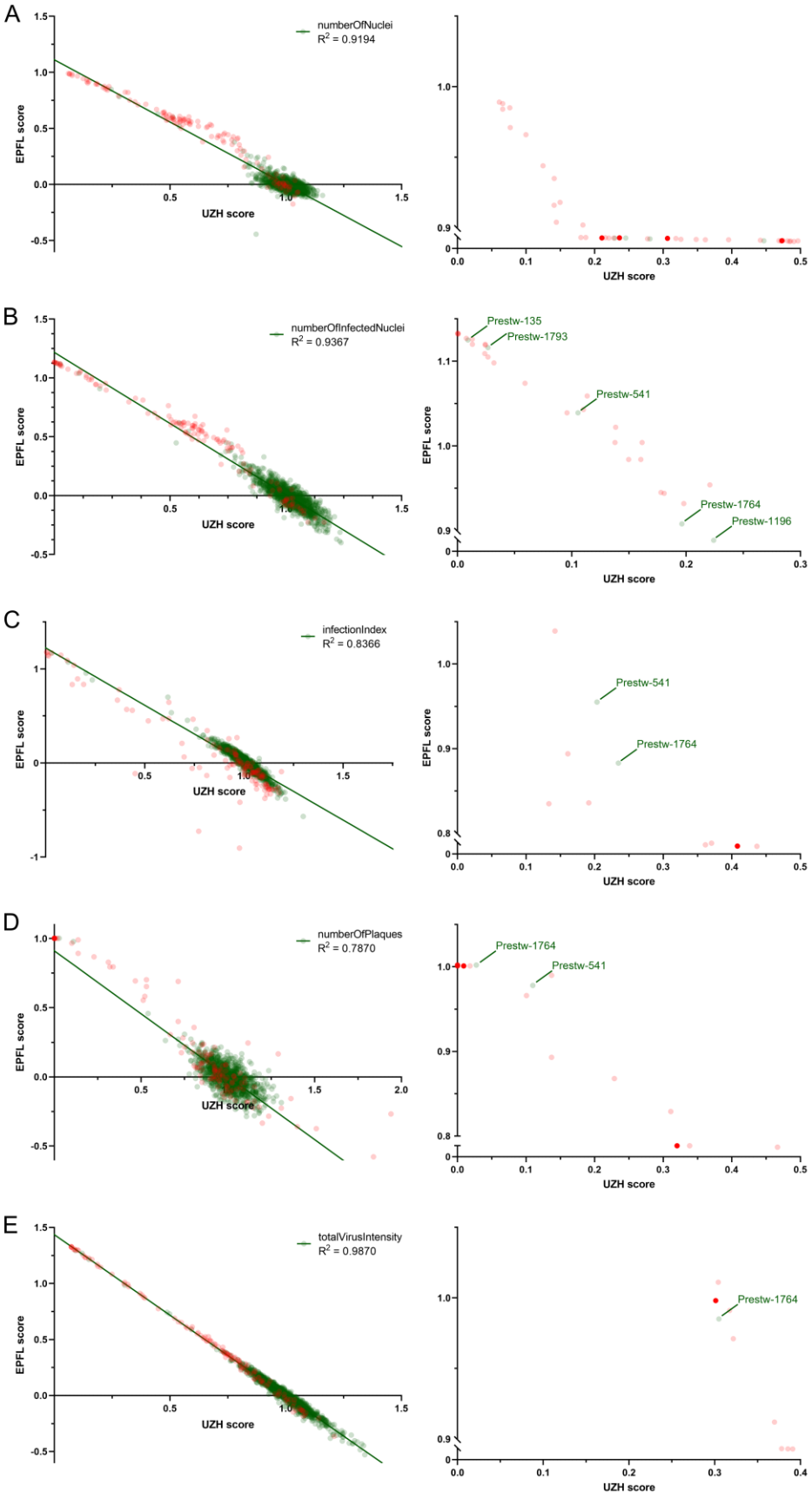

410

411 **Fig. 6: Correlation between PCL scores from independent dry-lab pipelines.** Imaging, image analysis
412 and data processing is performed independently at UZH and EPFL. PCL-treated infection phenotypes from
413 4 biological replicates were averaged and normalized against the DMSO solvent control. Obtained scores
414 for **A** *numberOfNuclei*, **B** *numberOfInfectedNuclei*, **C** *infectionIndex*, **D** *numberOfPlaques* and **E**
415 *totalVirusIntensity* of the 1,278 tested PCL compounds from UZH and EPFL are correlated via linear
416 regression (green line), R^2 is calculated using GraphPad Prism 8.2.1. Highest scoring compounds are
417 shown on the right and *PCL_ID* of non-toxic compounds indicated. Red dots indicate toxicity in the absence
418 of infection, non-toxic compounds are shown in green.

Tab. 1: Z'-factors of Z plates.

The quality of the screening platform is assessed prior to screening the PCL by two independent Z' plates containing 192 technical replicas of both positive control- (1.25 µM DFT) and negative solvent only control-treated (0.0125% DMSO). Z'-factors for the five Plaque2.0 read-outs [29] obtained by independent analysis at UZH and EPFL are calculated according to Equation 1 for 3 and 2σ.

		UZH					EPFL				
		3 sigma					3 sigma				
Barcode	Plate	numberOf Nuclei	numberOf Infected Nuclei	infection Index	numberOf Plaques	totalVirus Intensity	numberOf Nuclei	numberOf Infected Nuclei	infection Index	numberOf Plaques	totalVirus Intensity
BSF018104	Za	-1.11	0.50	0.57	0.50	0.07	-1.20	0.36	0.47	0.52	0.08
BSF018105	Zb	-8.10	0.30	0.45	0.39	-0.07	-1.23	0.27	0.32	0.44	-0.04
Mean		-4.61	0.40	0.51	0.44	0.00	-1.22	0.32	0.40	0.48	0.02

		UZH					EPFL				
		2 sigma					2 sigma				
Barcode	Plate	numberOf Nuclei	numberOf Infected Nuclei	infection Index	numberOf Plaques	totalVirus Intensity	numberOf Nuclei	numberOf Infected Nuclei	infection Index	numberOf Plaques	totalVirus Intensity
BSF018104	Za	-0.41	0.67	0.71	0.67	0.07	-0.47	0.58	0.64	0.68	0.38
BSF018105	Zb	-5.07	0.53	0.63	0.59	-0.07	-0.49	0.52	0.55	0.63	0.31
Mean		-2.74	0.60	0.67	0.63	0.00	-0.48	0.55	0.60	0.66	0.35

Tab. 2: Z'-factors of screening plates.

The quality of the screening data is quantified for each screening plate based on the 32 technical replicas of both positive control- (1.25 µM DFT) and negative solvent only control-treated (0.0125% DMSO) included in each plate. Z'-factors for the five Plaque2.0 read-outs [29] obtained by independent analysis at UZH and EPFL are calculated according to Equation (1) for 3σ.

		UZH					EPFL				
		3 sigma					3 sigma				
Barcode	Plate	numberOf Nuclei	numberOf Infected Nuclei	infection Index	numberOf Plaques	totalVirus Intensity	numberOf Nuclei	numberOf Infected Nuclei	infection Index	numberOf Plaques	totalVirus Intensity
BSF018292	1A	-0.13	0.58	0.58	0.59	0.35	-0.14	0.51	0.49	0.58	0.31
BSF018293	1B	-0.88	0.58	0.65	0.55	0.34	-0.35	0.51	0.52	0.51	0.35
BSF018294	1C	-1.01	0.62	0.62	0.63	0.33	-0.74	0.52	0.50	0.66	0.32
BSF018295	1D	-0.34	0.56	0.54	0.45	0.16	-0.21	0.43	0.38	0.46	0.19
BSF018296	2A	-1.35	0.64	0.67	0.55	0.30	-0.20	0.57	0.55	0.55	0.28
BSF018297	2B	-3.63	0.56	0.52	0.45	0.14	-1.20	0.45	0.39	0.40	0.12
BSF018298	2C	-1.81	0.60	0.58	0.49	0.24	-0.38	0.52	0.42	0.52	0.19
BSF018299	2D	-1.94	0.57	0.57	0.57	0.24	-0.22	0.50	0.43	0.63	0.20
BSF018300	3A	-1.74	0.64	0.66	0.56	0.36	-0.54	0.55	0.51	0.59	0.34
BSF018301	3B	-1.13	0.60	0.68	0.58	0.40	-0.09	0.52	0.57	0.59	0.40
BSF018302	3C	-4.02	0.66	0.68	0.48	0.42	-1.07	0.63	0.60	0.50	0.41
BSF018303	3D	-2.36	0.55	0.63	0.51	0.36	-0.10	0.58	0.54	0.52	0.35
BSF018304	4A	-0.68	0.70	0.74	0.42	0.37	-0.29	0.56	0.58	0.48	0.36
BSF018305	4B	-0.17	0.71	0.74	0.51	0.50	-0.50	0.63	0.67	0.50	0.50
BSF018306	4C	-0.44	0.61	0.62	0.50	0.28	-0.28	0.50	0.48	0.47	0.26
BSF018307	4D	-0.77	0.63	0.70	0.42	0.41	-0.22	0.54	0.56	0.36	0.39
Mean		-1.40	0.61	0.64	0.52	0.32	-0.41	0.53	0.51	0.52	0.31

Tab. 3: PCL compounds excluded due to toxicity in absence of infection. Presto-blue raw data is available at *ScreenA/4-Toxicity*.

PCL_ID	Compound	Score	ScoreSD	Toxic	PCL_ID	Compound	Score	ScoreSD	Toxic
Prestw-100	Nocodazole	0.75	0.02	yes	Prestw-347	Thioguanosine	0.18	0.03	yes
Prestw-1020	Rimexolone	0.39	0.08	yes	Prestw-353	Moclobemide	0.14	0.02	yes
Prestw-1040	Pyrvinium pamoate	0.74	0.03	yes	Prestw-362	Betamethasone	0.60	0.03	yes
Prestw-1044	Prednicarbate	0.54	0.00	yes	Prestw-363	Colchicine	0.91	0.00	yes
Prestw-1104	Clonixin Lysinate	0.22	0.05	yes	Prestw-373	Amethopterin (R,S)	0.20	0.01	yes
Prestw-1110	Parbendazole	0.40	0.02	yes	Prestw-377	Nafronyl oxalate	0.17	0.03	yes
Prestw-1119	Clocortolone pivalate	0.34	0.04	yes	Prestw-385	Mitoxantrone dihydrochloride	0.99	0.00	yes
Prestw-1134	Cytarabine	0.91	0.00	yes	Prestw-388	Dequalinium dichloride	0.46	0.00	yes
Prestw-1159	Sibutramine HCl	0.74	0.06	yes	Prestw-396	Etoposide	0.55	0.02	yes
Prestw-118	Nalbuphine hydrochloride	0.87	0.00	yes	Prestw-4	Metformin hydrochloride	0.12	0.00	yes
Prestw-1180	Docetaxel	0.86	0.03	yes	Prestw-409	Amiodarone hydrochloride	0.14	0.02	yes
Prestw-1196	Topotecan	0.62	0.04	yes	Prestw-419	Bisacodyl	0.15	0.01	yes
Prestw-1198	Tranilast	0.50	0.02	yes	Prestw-430	Cisapride	0.12	0.02	yes
Prestw-12	Benzonatate	0.85	0.06	yes	Prestw-432	Corticosterone	0.37	0.01	yes
Prestw-120	Triamcinolone	0.60	0.03	yes	Prestw-436	Digitoxigenin	0.99	0.00	yes
Prestw-1266	Gemcitabine	0.85	0.01	yes	Prestw-437	Digoxin	0.98	0.00	yes
Prestw-130	Dexamethasone acetate	0.53	0.02	yes	Prestw-438	Doxorubicin hydrochloride	0.96	0.00	yes
Prestw-1362	Vorinostat	0.19	0.01	yes	Prestw-439	Carbimazole	0.13	0.00	yes
Prestw-1408	Etoricoxib	0.20	0.03	yes	Prestw-447	Hydrocortisone base	0.55	0.02	yes
Prestw-1415	Floxuridine	0.15	0.04	yes	Prestw-448	Hydroxytacrine maleate (R,S)	0.11	0.00	yes
Prestw-1417	Fluconazole	0.42	0.01	yes	Prestw-456	Meclocycline sulfosalicylate	0.11	0.01	yes
Prestw-1419	Fluocinolone acetonide	0.60	0.03	yes	Prestw-457	Meclozine dihydrochloride	0.11	0.02	yes
Prestw-143	Chlorhexidine	0.19	0.02	yes	Prestw-458	Melatonin	0.13	0.01	yes
Prestw-1435	Melengestrol acetate	0.34	0.05	yes	Prestw-476	Primaquine diphosphate	0.16	0.01	yes
Prestw-1443	Misoprostol	0.54	0.05	yes	Prestw-478	Felodipine	0.16	0.01	yes
Prestw-1476	Amcinonide	0.62	0.02	yes	Prestw-48	Dicyclomine hydrochloride	0.13	0.03	yes
Prestw-1484	Cladribine	0.72	0.03	yes	Prestw-481	Serotonin hydrochloride	0.13	0.01	yes
Prestw-1486	Cortisol acetate	0.38	0.08	yes	Prestw-487	Daunorubicin hydrochloride	1.00	0.00	yes
Prestw-1509	Deflazacort	0.56	0.01	yes	Prestw-497	Vancomycin hydrochloride	0.12	0.02	yes
Prestw-155	Paclitaxel	0.88	0.02	yes	Prestw-498	Artemisinin	0.12	0.00	yes
Prestw-1704	Desonide	0.48	0.06	yes	Prestw-513	Norcyclobenzaprine	0.13	0.00	yes
Prestw-1712	Flumethasone pivalate	0.60	0.02	yes	Prestw-514	Pyrazinamide	0.11	0.01	yes
Prestw-1715	Algestone acetophenide	0.11	0.00	yes	Prestw-518	Budesonide	0.61	0.00	yes
Prestw-1722	Azatadine maleate	0.28	0.13	yes	Prestw-522	Thiostrepton	0.15	0.01	yes
Prestw-1740	Besifloxacin hydrochloride	0.36	0.09	yes	Prestw-529	Mesoridazine besylate	0.13	0.00	yes
Prestw-1741	Loteprednol etabonate	0.46	0.05	yes	Prestw-530	Trolox	0.16	0.00	yes
Prestw-1752	Epirubicin hydrochloride	0.90	0.02	yes	Prestw-553	Pentamidine isethionate	0.64	0.01	yes
Prestw-176	Iproniazide phosphate	0.21	0.11	yes	Prestw-572	Mometasone furoate	0.61	0.00	yes
Prestw-1761	Rizatriptan benzoate	0.43	0.00	yes	Prestw-6	Isoflupredone acetate	0.63	0.01	yes
Prestw-1801	Ciclesonide	0.55	0.03	yes	Prestw-619	Diflorasone Diacetate	0.61	0.00	yes
Prestw-1802	Darunavir	0.43	0.06	yes	Prestw-641	Sulmazole	0.44	0.01	yes
Prestw-192	Thalidomide	0.34	0.09	yes	Prestw-643	Flunisolide	0.64	0.01	yes
Prestw-20	Minoxidil	0.60	0.01	yes	Prestw-645	Flurandrenolide	0.64	0.01	yes
Prestw-200	Camptothecine (S,+)	0.69	0.02	yes	Prestw-652	Picrotoxinin	0.16	0.07	yes
Prestw-216	Tiapride hydrochloride	0.39	0.02	yes	Prestw-655	Halcinonide	0.60	0.01	yes
Prestw-217	Mebendazole	0.36	0.02	yes	Prestw-656	Lanatoside C	0.98	0.00	yes
Prestw-222	Antimycin A	0.53	0.08	yes	Prestw-718	Fluorometholone	0.55	0.03	yes
Prestw-223	Xylometazoline hydrochloride	0.22	0.09	yes	Prestw-72	Imipramine hydrochloride	0.55	0.00	yes
Prestw-226	Griseofulvin	0.37	0.07	yes	Prestw-734	Flumethasone	0.58	0.04	yes
Prestw-244	Glutethimide, para-amino	0.59	0.00	yes	Prestw-743	Medrysone	0.34	0.01	yes
Prestw-260	Praziquantel	0.57	0.05	yes	Prestw-771	Alclometasone dipropionate	0.55	0.02	yes
Prestw-268	Vinpocetine	0.41	0.01	yes	Prestw-774	Fluocinonide	0.55	0.03	yes
Prestw-271	Vincamine	0.25	0.00	yes	Prestw-777	Alexidine dihydrochloride	0.90	0.00	yes
Prestw-272	Indomethacin	0.41	0.00	yes	Prestw-781	Clobetasol propionate	0.63	0.00	yes
Prestw-273	Cortisone	0.57	0.01	yes	Prestw-782	Podophyllotoxin	0.89	0.00	yes
Prestw-274	Prednisolone	0.61	0.00	yes	Prestw-790	Cycloheximide	0.76	0.01	yes
Prestw-275	Fenofibrate	0.15	0.01	yes	Prestw-855	Beclomethasone dipropionate	0.52	0.02	yes
Prestw-279	Methylprednisolone, 6-alpha	0.61	0.00	yes	Prestw-883	Digoxigenin	0.94	0.00	yes
Prestw-299	Mifepristone	0.12	0.01	yes	Prestw-97	Disulfiram	0.81	0.04	yes
Prestw-318	Quinacrine dihydrochloride dihydrate	0.11	0.03	yes	Prestw-975	Naftopidil dihydrochloride	0.59	0.01	yes
Prestw-337	Procainamide hydrochloride	0.14	0.01	yes	Prestw-986	Proscillaridin A	0.98	0.00	yes
Prestw-339	Guanfacine hydrochloride	0.19	0.01	yes	Prestw-997	Fluticasone propionate	0.63	0.02	yes
Prestw-34	Triamterene	0.14	0.00	yes	Prestw-998	Zuclopenthixol hydrochloride	0.13	0.01	yes

434 **Tab. 4: Summary of screening controls and top hits. Compounds are scored toxic, if they show**
435 **significant toxicity in either of the assays.** Mean correspond to means over four biological replicates of
436 PCL compound and 16 biological replicates each carrying 16 technical replicates for each control. Neg. ctr.
437 refers to negative control (DMSO), pos. ctr. to positive control (DFT). Normalized indicates each com-
438 pound's mean read-outs relative to the mean of the positive control. Toxicity is accessed by presto-blue
439 assay of 72 h treatment of non-infected A549 cells as well as by the nuclei Z'-factor in the screen. Hits are
440 selected for low toxicity and high inhibitory effect compared to solvent control.

						Mean read-outs					Normalized mean read-outs					Hit			
PCL_ID	compound Identifier	Compound	Group	Toxic	Analysis	Nuclei	Infected nuclei	Infection index	Plaques	Virus intensity [AU]	Nuclei	Infected nuclei	Infection index	Plaques	Virus intensity [AU]	Nuclei	Infected nuclei	Infection index	Plaques	Virus intensity [AU]
DMSO	DMSO	DMSO	neg. ctr.	no	UZH	36'399	27'911	0.77	27.32	9.79E+09	1.00	1.00	1.00	1.00	1.00	-	-	-	-	-
					EPFL	29'749	15'156	0.51	21.11	5.02E+09	1.00	1.00	1.00	1.00	1.00					
DFT	DFT	DFT	pos. ctr.	no	UZH	30'204	3'595	0.12	0.12	2.90E+09	0.83	0.13	0.15	0.00	0.30	-	-	-	-	-
					EPFL	20'745	1'776	0.09	0.03	1.62E+09	0.70	0.12	0.17	0.00	0.32					
Prestw-1764	497	Nelfinavir mesylate	PCL	no	UZH	30'908	5'479	0.18	0.75	2.98E+09	0.85	0.20	0.23	0.03	0.30	no	yes	yes	yes	yes
					EPFL	21'895	2'988	0.14	0.00	1.68E+09	0.74	0.20	0.27	0.00	0.33	no	yes	yes	yes	yes
Prestw-388	763	Dequalinium dichloride	PCL	yes	UZH	28'763	13'751	0.48	14.00	3.62E+09	0.79	0.49	0.62	0.51	0.37	no	yes	yes	yes	yes
					EPFL	21'247	4'988	0.23	9.25	1.92E+09	0.71	0.33	0.46	0.44	0.38	yes	yes	yes	yes	yes
Prestw-1717	452	Aminacrine	PCL	no	UZH	31'723	14'689	0.47	20.50	4.88E+09	0.87	0.53	0.62	0.75	0.50	no	yes	yes	no	yes
					EPFL	42'191	9'057	0.22	14.25	2.54E+09	1.42	0.60	0.42	0.67	0.51	no	no	yes	no	yes
Prestw-925	1214	Thonzonium bromide	PCL	no	UZH	30'644	15'057	0.49	14.75	4.77E+09	0.84	0.54	0.63	0.54	0.49	no	yes	yes	no	yes
					EPFL	24'093	6'849	0.28	11.75	2.51E+09	0.81	0.45	0.56	0.56	0.50	no	yes	no	no	no

441

Suppl. Tab. 1: PCL compounds tested in the screening procedure. PCL catalogue IDs (*PCL_ID*), compound names (*CompoundName*) and spottability flag (*SpottabilityFlag*) for the 1,280 compounds of the PCL. Two compounds, namely Prestw-354 (Clopamide) and Prestw-410 (Amphotericine B) could not be successfully transferred via acoustic dispensing e.g. due to precipitation and were therefore not included in the screening.

Suppl. Tab. 2: UZH HAdV screening infection scores.

Suppl. Tab. 3: Scored UZH PCL-treated HAdV infection phenotype.

Suppl. Tab. 4: EPFL HAdV screening infection scores.

Suppl. Tab. 5: Scored EPFL PCL-treated HAdV infection phenotype.

References:

1. The Image Data Resource (IDR). *The Image Data Resource (IDR)* at <https://idr.openmicroscopy.org/>
2. Krilov, L. R. Adenovirus infections in the immunocompromised host. *Pediatr. Infect. Dis. J.* **24,** 555–556 (2005).
3. Greber, U. F., Arnberg, N., Wadell, G., Benkő, M. & Kremer, E. J. Adenoviruses - from pathogens to therapeutics: a report on the 10th International Adenovirus Meeting. *Cell Microbiol.* **15,** 16–23 (2013).
4. Tunkel, A. R., Baron, E. L., Buch, K. A., Marty, F. M. & Martinez-Lage, M. Case 31-2019: A 45-Year-Old Woman with Headache and Somnolence. *N. Engl. J. Med.* **381,** 1459–1470 (2019).
5. Gray, G. C. *et al.* Genotype prevalence and risk factors for severe clinical adenovirus infection, United States 2004-2006. *Clin. Infect. Dis.* **45,** 1120–1131 (2007).
6. Metzgar, D. *et al.* Abrupt emergence of diverse species B adenoviruses at US military recruit training centers. *J. Infect. Dis.* **196,** 1465–1473 (2007).
7. Lynch, J. P. & Kajon, A. E. Adenovirus: epidemiology, global spread of novel serotypes, and advances in treatment and prevention. *Semin Respir Crit Care Med* **37,** 586–602 (2016).
8. Haque, E., Banik, U., Monowar, T., Anthony, L. & Adhikary, A. K. Worldwide increased prevalence of human adenovirus type 3 (HAdV-3) respiratory infections is well correlated with heterogeneous hypervariable regions (HVRs) of hexon. *PLoS One* **13,** e0194516 (2018).
9. Ginn, S. L., Amaya, A. K., Alexander, I. E., Edelstein, M. & Abedi, M. R. Gene therapy clinical trials worldwide to 2017: An update. *J Gene Med* **20,** e3015 (2018).
10. Jiang, H. *et al.* Oncolytic adenovirus research evolution: from cell-cycle checkpoints to immune checkpoints. *Curr Opin Virol* **13,** 33–39 (2015).
11. Lawler, S. E., Speranza, M.-C., Cho, C.-F. & Chiocca, E. A. Oncolytic viruses in cancer treatment: A review. *JAMA Oncol.* **3,** 841–849 (2017).
12. Mennechet, F. J. D. *et al.* A review of 65 years of human adenovirus seroprevalence. *Expert Rev. Vaccines* **18,** 597–613 (2019).
13. Lion, T. Adenovirus persistence, reactivation, and clinical management. *FEBS Lett.* (2019). doi:10.1002/1873-3468.13576
14. Ismail, A. M. *et al.* Genomic foundations of evolution and ocular pathogenesis in human adenovirus species D. *FEBS Lett.* **593,** 3583–3608 (2019).
15. Harrach, B., Tarján, Z. L. & Benkő, M. Adenoviruses across the animal kingdom: a walk in the zoo. *FEBS Lett.* (2019). doi:10.1002/1873-3468.13687
16. Reddy, V. S., Natchiar, S. K., Stewart, P. L. & Nemerow, G. R. Crystal structure of human adenovirus at 3.5 A resolution. *Science* **329,** 1071–1075 (2010).
17. Benevento, M. *et al.* Adenovirus composition, proteolysis, and disassembly studied by in-depth qualitative and quantitative proteomics. *J. Biol. Chem.* **289,** 11421–11430 (2014).
18. Greber, U. F. & Flatt, J. W. Adenovirus entry: from infection to immunity. *Annu. Rev. Virol.* **6,** 177–197 (2019).
19. Bauer, M. *et al.* The e3 ubiquitin ligase mind bomb 1 controls adenovirus genome release at the nuclear pore complex. *Cell Rep.* **29,** 3785–3795.e8 (2019).
20. Prasad, V. *et al.* The UPR sensor IRE1α and the adenovirus E3-19Kglycoprotein sustain persistent and lytic infections. *Nat. Commun.* (2020).
21. Yakimovich, A. *et al.* Cell-free transmission of human adenovirus by passive mass transfer in cell culture simulated in a computer model. *J. Virol.* **86,** 10123–10137 (2012).
22. Tollefson, A. E. *et al.* The adenovirus death protein (E3-11.6K) is required at very late stages of infection for efficient cell lysis and release of adenovirus from infected cells. *J. Virol.* **70,** 2296–2306 (1996).
23. Doronin, K. *et al.* Overexpression of the ADP (E3-11.6K) protein increases cell lysis and spread of adenovirus. *Virology* **305,** 378–387 (2003).

24. Lenaerts, L. & Naesens, L. Antiviral therapy for adenovirus infections. *Antiviral Res.* **71,** 172–180 (2006).
25. Wold, W. S. M., Tollefson, A. E., Ying, B., Spencer, J. F. & Toth, K. Drug development against human adenoviruses and its advancement by Syrian hamster models. *FEMS Microbiol. Rev.* **43,** 380–388 (2019).
26. Wall, G. *et al.* Screening a Repurposing Library for Inhibitors of Multidrug-Resistant Candida auris Identifies Ebselen as a Repositionable Candidate for Antifungal Drug Development. *Antimicrob. Agents Chemother.* **62,** (2018).
27. Chauvin, C. *et al.* High-Throughput Drug Screening Identifies Pazopanib and Clofilium Tosylate as Promising Treatments for Malignant Rhabdoid Tumors. *Cell Rep.* **21,** 1737–1745 (2017).
28. Prestwick Chemical publications. *Prestwick Chemical publications* at <http://www.prestwickchemical.com/libraries-publications.html>
29. Yakimovich, A. *et al.* Plaque2.0-A High-Throughput Analysis Framework to Score Virus-Cell Transmission and Clonal Cell Expansion. *PLoS One* **10,** e0138760 (2015).
30. Greber, U. F., Willetts, M., Webster, P. & Helenius, A. Stepwise dismantling of adenovirus 2 during entry into cells. *Cell* **75,** 477–486 (1993).
31. R Core Team. *R:A Language and Environment for Statistical Computing*. (R Foundation for Statistical Computing, 2018).
32. Berthold, M. R. *et al.* KNIME - the Konstanz information miner. *SIGKDD Explor. Newsl.* **11,** 26 (2009).